Supporting Information for "Southern Ocean Ice-Covered Eddies Properties From Satellite Altimetry"

Matthis Auger[1,2,3], Jean-Baptiste Sallée[3], Andrew F. Thompson[4], Etienne Pauthenet[3,5], Pierre Prandi[6]

[1]Insitute for Marine and Antarctic studies, University of Tasmania, Hobart, Australia

[2]The Australian Centre for Excellence in Antarctic Science, University of Tasmania, Hobart, Australia

[3]Sorbonne Université, CNRS, LOCEAN, Paris, France

[4]Environmental Sciences and Engineering, California Institute of Technology, Pasadena, CA, USA

[5]Ifremer, Univ. Brest, CNRS, IRD, Laboratoire d'Océanographie Physique et Spatiale (LOPS), IUEM, 29280, Plouzané, France.

[6]Collecte Localisation Satellite, Toulouse, France

Contents of this file

1. Figure S1: Sensitivity study of the maps of mean amplitudes and frequency.

2. Figure S2: Sensitivity study of the density of the eddies as a function of the Sea Ice Concentration (SIC).

3. Figure S3: Sensitivity study of the amplitude of the eddies as a function of the Sea Ice Concentration (SIC)

4. Figure S4: Number of along track data per gridpoint and spatial scale resolved.

5. Figure S5: Number of along track measurements within the contour of the eddies as a function of sea ice concentration.

Introduction

The supplementary information presented here provides more insights into the results described in the main paper. We are conscious that there are many unknowns on the capacities of the observation dataset for the observation of mesoscale eddies under sea ice, even more considering the small Rossby radius of the region (Chelton et al., 2011). This supporting information provides more insights into the robustness of the results presented here and into the spatial scales resolved by the dataset.

1. Sensitivity study

As stated in the paper, we have been concerned by both the effects of the possible artifacts of the dataset and its resolution. We decided to tackle these issues by reproducing some of the diagnostics of the paper, either by selecting only the eddies with an amplitude larger than the error estimated in the seasonally ice-covered regions or by subsampling the along-track measurements upstream of the mapping of the Sea Level Anomaly dataset and the eddy detection process. We therefore define two experimental cases:

- The "All" case is the original case. We kept all the eddies and all the along-track measurements before the mapping.

- The "Amp" case. In this case, we remove all the eddies with amplitudes lower than the mean error of the ice-covered regions (Auger, Sallée, et al., 2022, i.e. 3.7cm).

- The "Samp" case. In this case, the along-track measurements have been subsampled before the mapping of the product presented in (Auger, Prandi, & Sallée, 2022). We sampled the AltiKa and Sentinel-3A to reach 1 Hz measurements in the ice-free ocean.

In the ice-covered measurements, we only kept 1 valid point out of 3 for Sentinel-3A and Crysosat-2, and 1 out of 6 for AltiKa, as it is emitting twice more measurements compared to the formers. These values were chosen arbitrarily to find a compromise between downgrading the dataset and not flattening all the signal. Other sampling frequencies were not tested as the computation of a new dataset requires lots of time and computing power. After this subsampling, we constructed the dataset the same way as its unsampled, original version. We then applied the detection and tracking method.

Figure S1 shows the maps of the mean eddy amplitudes and frequencies. The spatial pattern of eddy amplitude is rather consistent between all the cases. The amplitudes are distributed the same way for all the cases (Figure S1a-c), but with unsurprisingly stronger amplitudes in the Amp case. The amplitude in the Samp case is a little lower than in the All case, showing a slight flattening effect of having fewer measurements. One point of the paper is the uniform distribution of the eddies in the subpolar basin. Figure S1d-e shows how this changes between the various cases. The eddy frequency in the Amp case is twice as small as the All case. This shows that a large part of the eddies detected has an amplitude lower than the estimated error of the dataset. In the Amp case, the density is less uniform as there are stronger eddies in the northern extent of the subpolar region, where the mesoscale activity is enhanced by the neighboring ACC. In the Samp case, the frequency is uniform and higher than in the All case. Amores, Jordà, Arsouze, and Sommer (2018) pointed that lower resolution along-track measurements upstream of the mapping of ocean topography may induce larger eddies, as the interpolation would spread the signal further. In this study, we decided to not focus on the radius as it is one of the eddy properties the most impacted by varying resolution of the input dataset. In

this case, the higher frequency may be explained by larger eddies covering more pixels, thus increasing the chances for a gridpoint to be contained into an eddy.

Figure S2 shows the sensitivity of the density of the eddies as a function of sea ice concentration. The distributions of the three cases are similar and show higher densities in the northern-MIZ, but with lower densities for both experimental cases. In the Amp case, the dominance of cyclones over and anticyclonic eddies is even larger than the ALL case, with cyclones density reaching twice the one of anticyclones in SIC between 20 and 30%. Interestingly, the overall dominance of the eddy density in the n-MIZ is smaller in the Samp case, as the diminishing number of cyclones is compensated by a growing number of anticyclones. We do not have explanations for this growing density of cyclones with SIC when subsampling the dataset.

Figure S3 shows the distribution of the median density of the eddies as a function of sea ice concentration for all the cases. Once again the distribution is similar, with larger eddies in the MIZ than in the pack ice. However, when selecting only the strongest eddies (Amp), the maximum density is found in both the southern and northern MIZ, between 20 and 50 % of SIC, and cyclonic eddies at their maximum amplitude even up to 60% of SIC. This does not change the conclusions of our study. Figures S1, S2, and S3 show that our results are robust to the impact of the small eddies and to the resolution of the measurements used.

2. Spatial scales resolved

We are conscious that knowing accurately the spatial scales resolved will probably go through the computation of the effective resolution of the dataset, which has not been engaged at the moment. To have a first hint of the scales resolved, we show Figure S4 the

mean number of observations per pixel in 10 days intervals in winter and summer seasons, and the associated mean spatial scales resolved. There are on average more than 100 observations per pixel in the ice-free ocean and more of the order of 10 observations per pixels in the ice-covered ocean (Figure S4ab). The number of observations does not seem to decrease with increasing sea ice concentration. In fact, the potentially lower number of leads may be compensated by the tightened satellite tracks, allowing the finding of a higher fraction of the leads. Figures S4cb show the associated mean spatial scale resolved. It has been computed as $\sqrt{\frac{625}{nb\_pts}}$, 625 km^2 being the surface of a grid cell. It is computed as a proxy of the spatial resolution of the product. This spatial scale about 1 kilometer in the ice-free ocean, and closer to 10 kilometers in the ice-covered ocean, of the order of the local Rossby Radius in the subpolar Southern Ocean (Chelton et al., 1998).

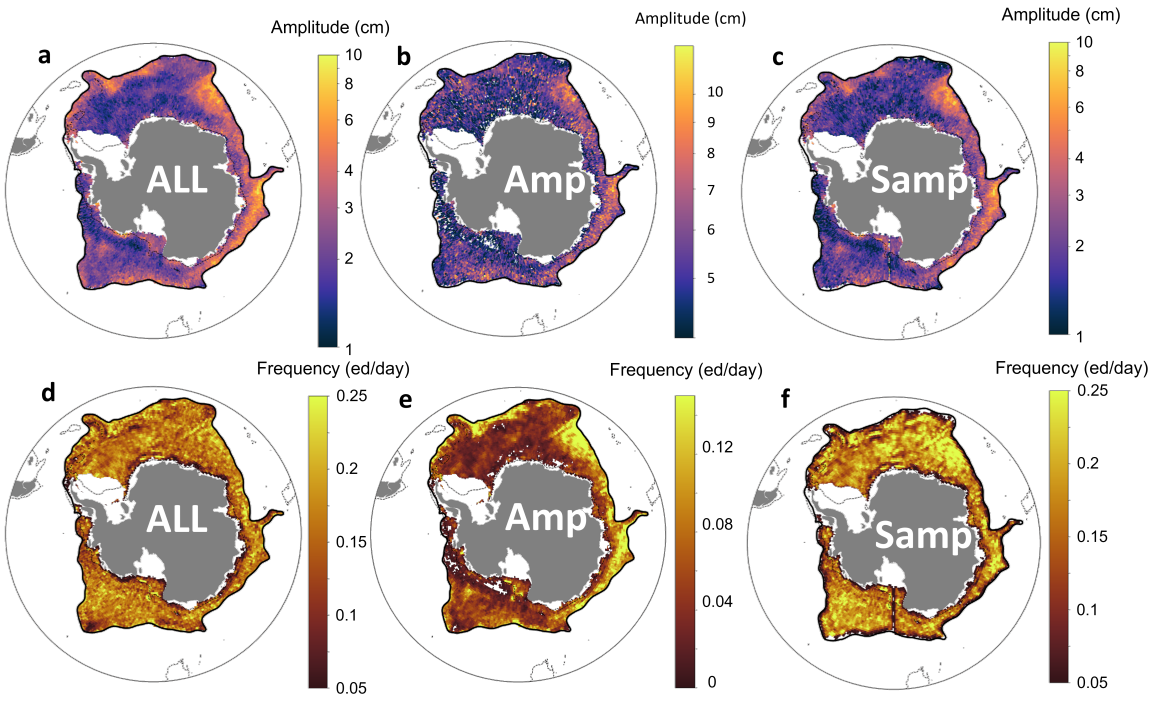

Figure S1. Sensitivity study of the maps of mean amplitudes and frequency. The first line (a-c) shows the map of the mean amplitude of the tracked eddy for each sensitivity study. The second line (d-f) shows the map of the frequency of the days the pixels are located into an eddy. The first row (a,d) is the case presented in this study containing all the eddies (ALL case). The second row (b,e) is the case for which only the eddies with an amplitude larger than 3.7 centimeters are included in the calculation (Amp case). The last row (c,f) is the case for which the along-track data was subsampled before the mapping of the Sea Level Anomaly product (Samp). The black dashed line is the -1000m isobath. The bold black line is the limit of the subpolar Southern Ocean as defined in this study.

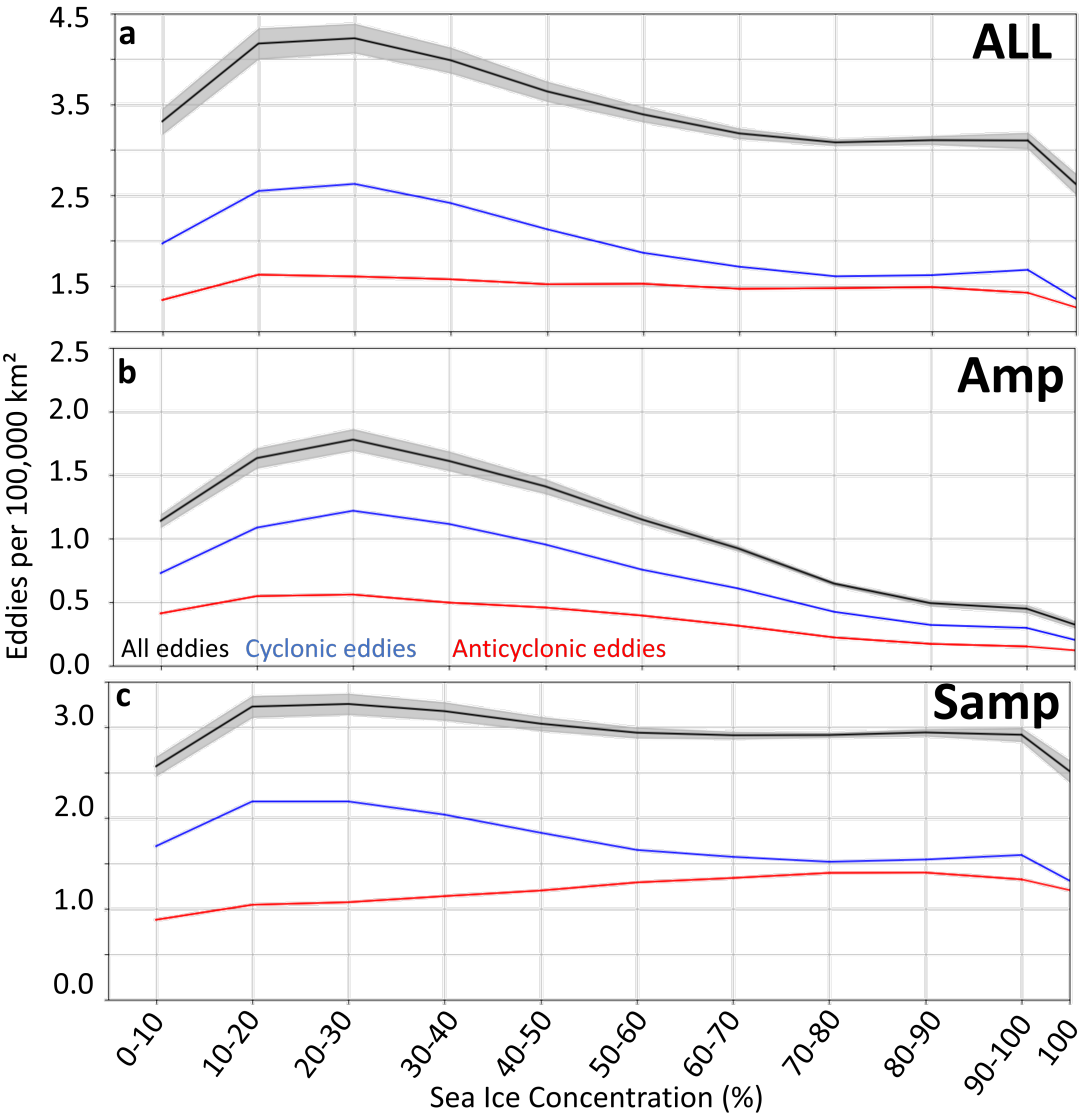

Figure S2. Sensitivity study of the density of the eddies as a function of the Sea Ice Concentration (SIC). The black curve is the density of all the eddies, the blue one is the density of the cyclonic eddies and the red one is the density of the anticyclonic eddies (red) as a function of the sea ice cover. (a) is the case presented in this study containing all the eddies (ALL case). Panel (b) is the case for which only the eddies with an amplitude larger than 3.7 centimeters are included in the calculation (Amp case). Panel(c) is the case for which the along-track data was subsampled before the mapping of the Sea Level Anomaly product (Samp).

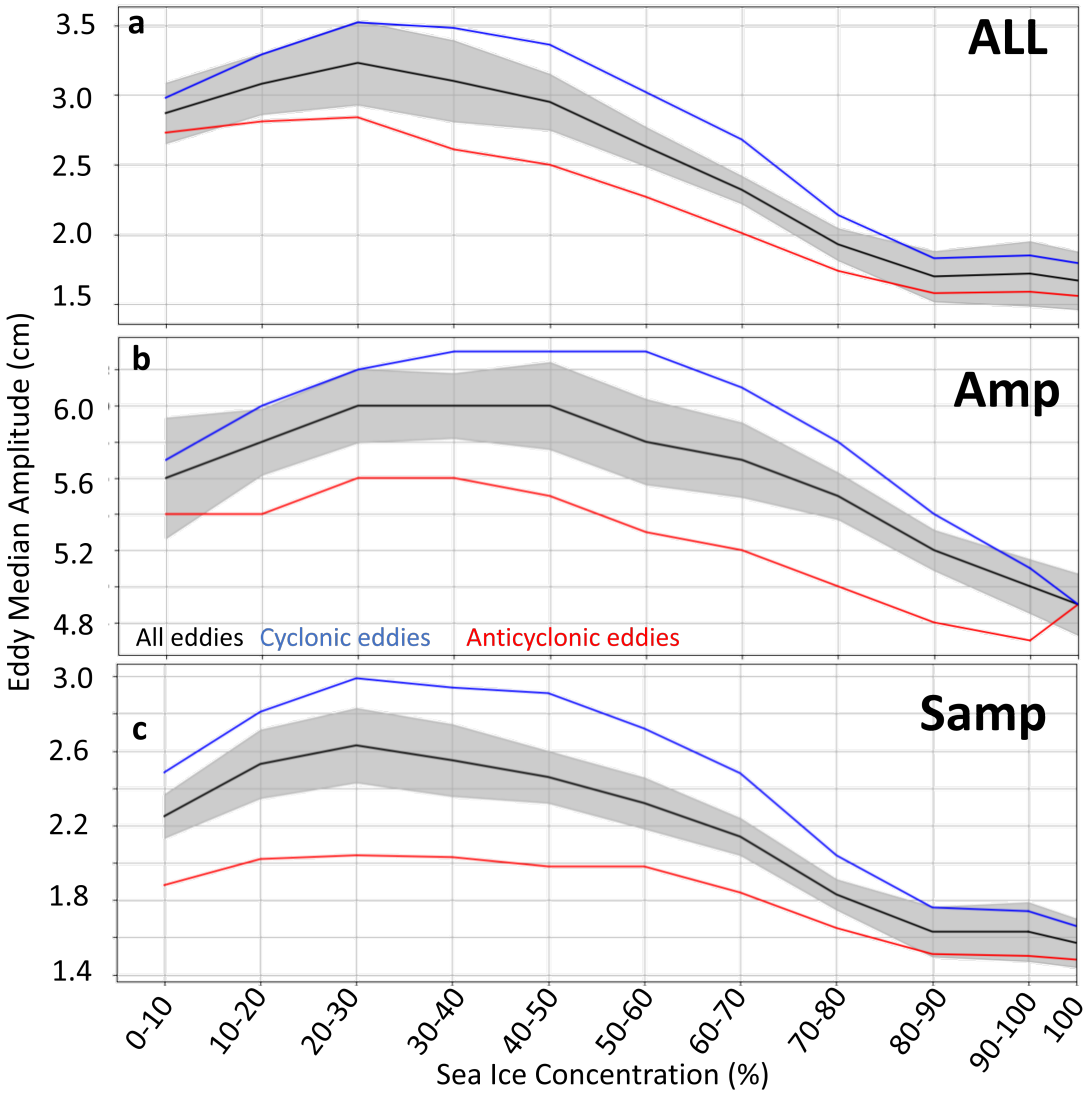

Figure S3. Sensitivity study of the amplitude of the eddies as a function of the Sea Ice Concentration (SIC). The black curve is the median amplitude of all the eddies, the blue one is the median amplitude of the cyclonic eddies and the red one is the median amplitude of the anticyclonic eddies (red) as a function of the sea ice cover. (a) is the case presented in this study containing all the eddies (ALL case). Panel (b) is the case for which only the eddies with an amplitude larger than 3.7 centimeters are included in the calculation (Amp case). Panel (c) is the case for which the along-track data was subsampled before the mapping of the Sea Level Anomaly product (Samp).

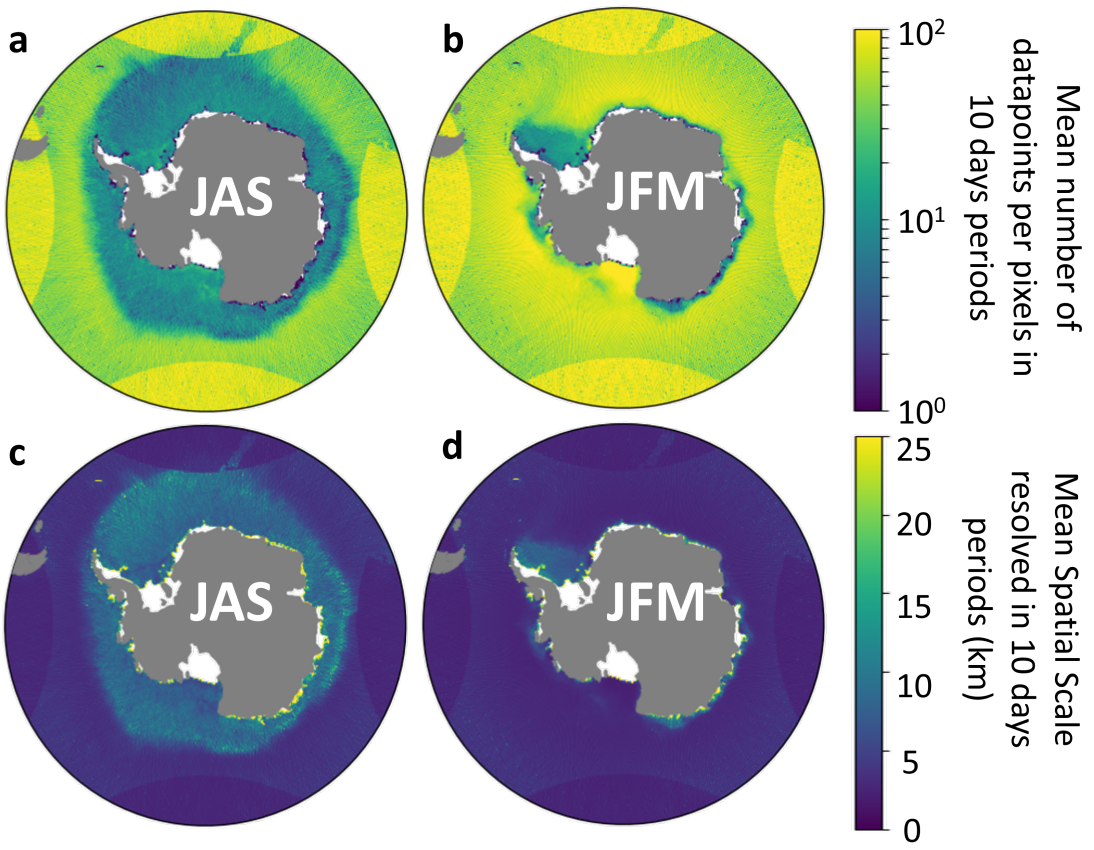

Figure S4. (a,b) Mean number of data in 10 days intervals for Winter (JAS, July, August, September) and Summer (January, February, March). (c,d) Mean spatial scale resolved in 10 days periods in Winter and Summer. The mean spatial scale resolved is computed as $\sqrt{\frac{625}{nb\_pts}}$, 625 km^2 being the surface of a grid cell.

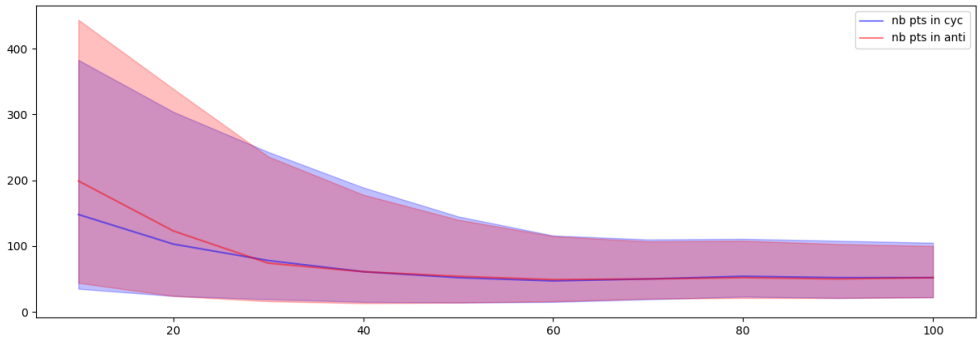

Figure S5. Number of along track measurements within the contour of the cyclones (blue) or the anticyclones (red) as a function of the sea ice concentration. The shading represents the 25 and 75 percentiles.

References

Amores, A., Jordà, G., Arsouze, T., & Sommer, J. L. (2018). Up to What Extent Can We Characterize Ocean Eddies Using Present-Day Gridded Altimetric Products? *Journal of Geophysical Research: Oceans*, *123*(10), 7220–7236. Retrieved 2021-07-21, from https://agupubs.onlinelibrary.wiley.com/doi/abs/10.1029/2018JC014140 (_eprint: https://agupubs.onlinelibrary.wiley.com/doi/pdf/10.1029/2018JC014140) doi: 10.1029/2018JC014140

Auger, M., Prandi, P., & Sallée, J.-B. (2022, March). Southern ocean sea level anomaly in the sea ice-covered sector from multimission satellite observations. *Scientific Data*, *9*(1), 70. Retrieved 2022-03-07, from https://www.nature.com/articles/s41597-022-01166-z (Number: 1 Publisher: Nature Publishing Group) doi: 10.1038/s41597-022-01166-z

Auger, M., Sallée, J.-B., Prandi, P., & Naveira Garabato, A. C. (2022). Subpolar Southern Ocean Seasonal Variability of the Geostrophic Circulation From Multi-Mission Satellite Altimetry. *Journal of Geophysical Research: Oceans*, *127*(6), e2021JC018096. Retrieved 2022-06-28, from https://onlinelibrary.wiley.com/doi/abs/10.1029/2021JC018096 (_eprint: https://onlinelibrary.wiley.com/doi/pdf/10.1029/2021JC018096) doi: 10.1029/2021JC018096

Chelton, D. B., deSzoeke, R. A., Schlax, M. G., Naggar, K. E., & Siwertz, N. (1998, March). Geographical Variability of the First Baroclinic Rossby Radius of Deformation. *Journal of Physical Oceanography*, *28*(3), 433–460. Retrieved 2021-07-13, from https://journals.ametsoc.org/view/journals/phoc/28/3/1520-0485_1998_028_0433_gvotfb_2.0.co_2.xml (Publisher: American Meteorological Society Section: Journal of Physical Oceanography) doi: 10.1175/1520-0485(1998)028⟨0433:GVOTFB⟩2.0.CO;2

Chelton, D. B., Schlax, M. G., & Samelson, R. M. (2011, October). Global observations of nonlinear mesoscale eddies. *Progress in Oceanography*, *91*(2), 167–216. Retrieved 2021-07-08, from https://www.sciencedirect.com/science/article/pii/S0079661111000036 doi: 10.1016/j.pocean.2011.01.002